

## Wave chaos in elastodynamic cavity scattering

A. Wirzba<sup>1</sup>, N. S. Jørgensen<sup>2</sup> and P. Cvitanovic<sup>3</sup><sup>1</sup> Institut für Kernphysik, Forschungszentrum Jülich – D-52425 Jülich, Germany<sup>2</sup> Matematisk Fysik, Lunds Universitet – Box 118, SE-22100 Lund, Sweden<sup>3</sup> Center for Nonlinear Science, School of Physics, Georgia Institute of Technology – Atlanta, GA 30332-0430, USA

PACS.05.45.Mt { Quantum chaos; semiclassical methods.

PACS.46.40.Cd { Mechanical wave propagation (including diffraction, scattering, ...).

PACS.62.30.+d { Mechanical and elastic waves; vibrations.

Abstract. { Exact elastodynamic scattering resonances are calculated for one- and two-cylindrical cavity systems, and compared to a elastodynamic generalization of the semiclassical Gutzwiller unstable periodic orbits formulas. In contrast to quantum mechanics, here complex periodic orbits associated with the surface Rayleigh waves dominate the low-energy spectrum, and already the two-cavity system displays chaotic features. The shortest of these orbits suffice to interpret the Wigner time delays and the leading elastodynamic scattering resonances.

Introduction. { The Gutzwiller semiclassical quantization of classically chaotic systems relates quantum observables such as spectral densities to sums over classical unstable periodic orbits [1,2]. The work presented here is a step toward a formulation of such approximate short-wavelength theory of wave chaos for the case of linear elastodynamics. Why elastodynamics? The elastodynamic experiments initiated by Oxborrow et al. [3] attain  $Q$  values as high as  $5 \times 10^6$  making spectral measurements in elastodynamics competitive with measurements in microwave cavities at liquid helium temperatures [4,5], and vastly superior to nuclear physics and room temperature microwave experiments for which the  $Q$  values are orders of magnitude lower, typically  $10^2$ – $10^3$ . So far, for elastodynamics there are only a few experimental demonstrations [6] of the existence of unstable periodic orbits, and no theory that would predict them. While Oxborrow et al. measure about  $10^5$  spectral lines, the current theory is barely adequate for computation of dozens of resonances. A more effective theory would find many applications such as in the frequency domain quality testing for small devices built from high  $Q$  materials. This unsatisfactory state of affairs is the *raison d'être* for the theoretical effort undertaken here.

While current experiments excel in measurements of eigenspectra of compact resonators, the periodic orbit theory computations of such bound system spectra are rendered difficult by presence of non-hyperbolic phase space regions. As our primary goal is to derive and test rules for replacing wave mechanics by the high-frequency ray-dynamic trajectories, we concentrate here instead on the problem of scattering of cylindrical cavities, for which the classical dynamics is fully under control.

In the case of one cavity the exact scattering spectrum is known [7]. For the multiple-cavities case we generalize here the quantum-mechanical S-matrix formalism for N-disk scattering [8,11], and compute the exact resonances and the Wigner time delays from the full elastodynamic wave-mechanical scattering matrix. We then compare the exact results with the corresponding quantities calculated in the short-wavelength approximation, and discover that the quantum-mechanical intuition fails us: the Rayleigh surface waves (which have no analog in the quantum scattering problem) dominate the low-energy spectrum, such that already the two-disk elastodynamic scattering problem displays chaotic features in this regime.

Elastodynamics. Consider an infinite slab of an isotropic and homogeneous elastic material (e.g., polyethylene or isotropic quartz) with parallel top and bottom plane boundaries, and an in-phase stimulus such that the system behaves quasi-two-dimensionally along the slab, with no excitation of or coupling to waves propagating perpendicular to the slab. The propagating waves are either the pressure or the shear solutions of the Navier-Cauchy equation [12]

$$\nabla^2 u + (\lambda + \mu)^{-1} \nabla(\nabla \cdot u) - \rho^{-1} \omega^2 u = 0; \tag{1}$$

where  $u$  is a vectorial displacement field, and  $\lambda, \mu$  are the Lamé constants,  $\rho$  the mass density and  $\omega$  the frequency. The experiments dictate free boundary conditions, with vanishing (vectorial) traction  $t(u) = 0$  where

$$t(u) = \lambda \nabla \cdot u \mathbb{1} + \mu \nabla u + \mu \nabla u^T \cdot \hat{n}; \tag{2}$$

Here  $\hat{n}$  is a unit vector normal to the boundary,  $\mathbb{1}$  the unit matrix, and  $T$  indicates a transposition. Elastodynamic waves are vectorial, with the pressure (longitudinal {L}) wave propagating through the bulk with velocity  $c_L = (\lambda + 2\mu)^{-1/2}$ , and the shear (transverse {T}) wave with velocity  $c_T = \mu^{-1/2}$ . Furthermore, the Rayleigh surface waves propagate along plane boundaries unattenuated, with the velocity  $c_R$  determined [12] by the condition

$$0 = 2^2 - 1^2 - 4^2 \frac{q}{(\lambda + 2\mu)(\lambda + \mu)} \text{ with } q = c_R^2; \tag{3}$$

When either a shear or pressure plane wave hits a boundary, mode conversion can take place [13], with waves of different types emitted at different angles. We now drill one, two, or more cylindrical cavities of radius  $a$  perpendicularly through the slab.

One-cavity scattering, the exact spectrum. Scattering of a single cylindrical cavity is separable in angular momentum. The one-cavity S-matrix of elastodynamics, a  $[2 \times 2]$  matrix in fL;Tg components, is determined by the free boundary condition for the traction matrices

$$S_{mm}^{(1)} = \frac{t_m^{(+)} t_m^{(-)}}{t_m^{(+)} t_m^{(-)}}; \quad m = 0; 1; 2; \dots; \tag{4}$$

For comparison, the corresponding one-disk scattering matrix [11,14] of quantum mechanics (QM), for a scalar field with the Dirichlet boundary condition, is expressed in terms of Hankel functions,  $S_{mm}^{(1)} = \frac{H_m^{(+)}(ka)}{H_m^{(-)}(ka)} = H_m^{(+)}(ka)$ , as function of the wave number  $k$ . The traction matrices [15] of angular momentum  $m$  and superscript  $Z \in \{+, -\}$ ; Jg result when outgoing (+), incoming (-) or regular (J) pressure and shear displacements  $u$  in terms of Hankel or Bessel functions,  $Z_m \in \{H_m^{(+)}; H_m^{(-)}; J_m\}$ , are inserted into the traction (2):

$$t_m^{(Z)} = \frac{2}{a^2} (\lambda + \mu) k \frac{d}{dk} \left[ m^2 \frac{1}{2} k_T^2 a^2 \text{Im}(1 - \dots) k \frac{d}{dk} \dots \right]; \tag{5}$$

Index  $2l; 2g$  labels the 2-d spherical components  $f_l; \hat{g}$  of the displacement  $u$  at the cavity while  $l; g$  labels its polarization  $f_l; Tg$  where  $k = \omega/c$  are the corresponding wave numbers. The scattering resonances for the one-cavity elastodynamic medium with traction-free boundary conditions are determined [7] from  $\text{Det } t_m^{(+)} = 0$ , see eq. (4).

Multi-cavity scattering, exact spectrum. { We construct the S-matrix for the N-cavity system following ref. [11]. The determinant of the N-scatterer S-matrix factorizes, as in QM, into the product of the one-cavity determinants and the multi-scattering contributions [11,15]:

$$\text{det } S(\omega) = \prod_{j=1}^N \text{det } S^{(1)j}(\omega) \frac{\text{Det } M(\omega)^N}{\text{Det } M(\omega)} \quad (6)$$

Here the matrix  $M = 1 + A$  is the inverse of the multi-scattering matrix. The transfer matrix  $A$  evolves the displacement of internal angular momentum  $l^0 = 0; 1; 2; \dots$  and spherical component  $g^0$  at cavity  $j^0$  (of radius  $a_{j^0}$ ) to the  $l = 0; 1; 2; \dots$  and  $2l; 2g$  displacement at cavity  $j$  (of radius  $a_j$ ) where  $j; j^0 = 1; \dots; N$  are the cavity-labels:

$$A_{ll^0}^{jj^0} = (1 - \delta_{jj^0}) \frac{a_j}{a_{j^0}} \frac{X^2}{X^2 - 1} t_1^{(j)j^0} T_{ll^0}^{(+ )jj^0} t_1^{(+ )jj^0} \quad (7)$$

$$T_{ll^0}^{(+ )jj^0} = H_{l+1}^{(+)}(kR_{jj^0}) \exp[i(l - j^0) \phi_{jj^0}] \quad (8)$$

The matrix  $T^{(+ )jj^0}$  translates the  $l; Tg$  modes evaluated relative to the origin of cavity  $j^0$  to the corresponding modes at cavity  $j$ , and  $R_{jj^0}$  and  $\phi_{jj^0}$  are the relative center-to-center distances and angles, respectively [11,15].

The genuine multi-scattering resonances of the N-cavity problem are given by the zeros of  $\text{Det } M(\omega)$ , see eq. (6).

For the two-cavity system the two-fold reflection symmetry implies that the determinant factors into four irreducible representations, with the transfer matrix for each irreducible subspace defined on the fundamental domain, a quarter of the full elastodynamic slab [2].

Here we present a few typical numerical results for the fully symmetric  $A_1$  subspace of the system of two cylindrical cavities. In all calculations reported here we take values of the Lamé constants corresponding to polyethylene [7], and set  $c_L = 1950 \text{ m/s}$ ,  $c_T = 540 \text{ m/s}$ ,  $c_R = 513 \text{ m/s}$ , and take cavities of radius  $a = 1 \text{ cm}$ , center-to-center separation  $R = 6 \text{ cm}$ . The lowest few hundred exact  $A_1$  resonances determined by the zeros of  $\text{Det}(1 + A)_{A_1}$  are shown in Fig. 1.

One-cavity scattering, ray-dynamic interpretation. { In the one-cavity case a sophisticated theory of ray dynamics already exists. The main tool is the Sommerfeld-Watson transformation which in the QM case replaces a slowly converging partial wave sum by a fast converging sum over complex creeping trajectories, first derived by Franz [14]. The pressure and shear Franz resonances also exist in elastodynamics [16], but here the one-cavity spectrum is dominated by the weakly damped Rayleigh resonances [7], with no QM counterpart.

In the spirit of Keller's geometrical theory of diffraction [16] we use the one-cavity S-matrix (4) to assign a ray-dynamic weight to a segment of the boundary traversed by a Rayleigh wave. A circular Rayleigh segment of arc length  $a$  (with the pertinent angle) has the complex-valued weight  $\exp[i k_T R(\omega)]$ , such that the effective arc length of a Rayleigh segment is  $R(\omega) = k_T^{-1} a$ , where  $k_T = c_T/c_R$ , see eq. (3). Here we take times the exact wave-mechanical  $R(\omega)$ , determined as complex angular momentum by  $\text{Det } t_R^{(+)}(\omega) = 0$ , as the input for the complex-valued action of the Rayleigh trajectory segment.

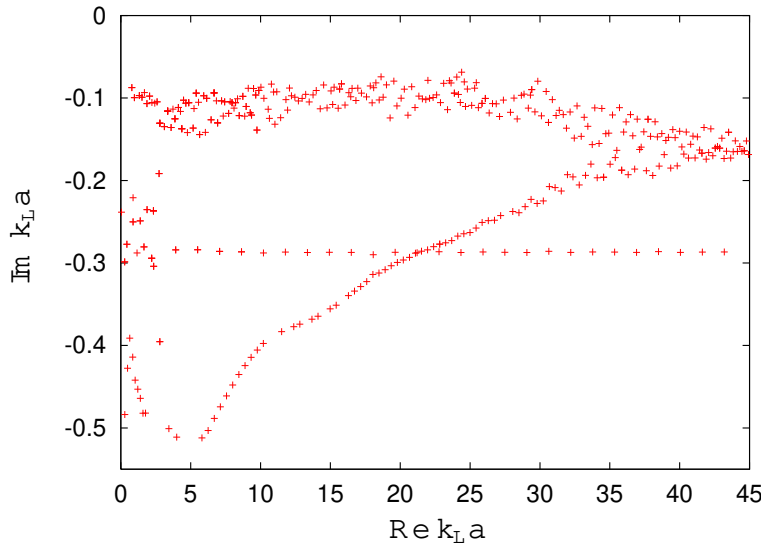


Fig. 1 { The lowest few hundred exact  $A_1$  resonances of the two-cavity elastodynamic scatterer, in the complex pressure wave number  $k_L = \omega/c_L$  plane (in units of the inverse of the cavity radius  $a$ ).

Multi-cavity scattering, ray-dynamic interpretation. { In QM the Gutzwiller-Voros Zeta function is the semi-classical approximation to  $\text{Det}M$ , where the connection follows via the semi-classical reduction of the traces  $\text{Tr}A^n$  appearing in the cumulant expansion

$$\text{Det}M = 1 + \text{Tr}A + \frac{1}{2} \text{Tr}A^2 + \dots + \text{Tr}A^n + \dots \quad (9)$$

As shown in refs. [10,11], in the short-wavelength approximation (SWA) the traces  $\text{Tr}A^n$  reduce to the set of ray-dynamic periodic orbits of topological length  $n$ , whereas the cumulants become "curvatures" (periodic orbits shadowed by pseudo orbits [2]). The shortest geometrical periodic orbits, bouncing between the two cavities, are the border orbits of topological length one in the fundamental domain. Their weights, derived from the SWA to  $\text{Tr}A_{A_1}$ , are of form [1,15]  $w_j = \exp i k (R - 2a) = \frac{1}{j_0} (1 - \frac{2a}{R})^j$  with  $j_0 = R - a + \frac{p}{R^2} 2Ra = a, 2fl; 2g - fl; Tg$ . These unstable geometrical orbits including their repetitions are summed up in the usual way in terms of the Gutzwiller-Voros spectral determinant  $\text{Det}M_{\text{geom}}$ : [2]. Moreover, Keller's theory yields orbits with unstable geometrical legs and weakly attenuated Rayleigh surface wave arcs circling the cavities. At the topological length one, two (unstable) complex Rayleigh-type periodic orbits, an "oval" and "figure eight" contribute [10]. In addition to the repeated primary orbits and the "oval" and "figure eight" combination, two further (unstable) Rayleigh-type orbits contribute to  $\text{Tr}A^2$ , see g. 2, and so on for longer periodic orbits. Note that the number of Rayleigh-type orbits grows exponentially with increasing topological order.

By analogy to creeping orbits [17,18], if  $q_i, i = 1; n$  (with  $q_i = q_i$ ) are the points along a cycle where a Rayleigh arc segment connects to geometric trajectories (which may include reflections with/without conversions between pressure and shear rays), the Rayleigh

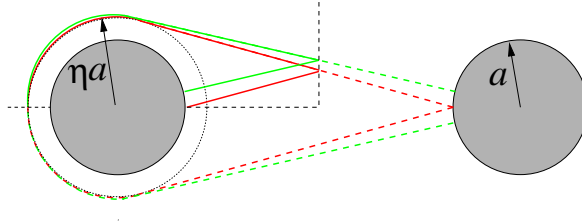


Fig. 2 { Two periodic orbits of Rayleigh type of topological length 2 (and "effective" arc radius  $a > a$ ), in the full space, and in the fundamental domain of the two-cavity system .

surface wave contribution to the spectral determinant is of form

$$\text{DetM}_{\text{Rayl}} = \exp \sum_{p;r=1}^{\infty} \frac{1}{r} \sum_{i=1}^{\infty} \#_r [G(q_{i+1}; q_i)]_{i+1, i} : \quad (10)$$

Here the summation goes over all prime periodic orbits  $p$  and their repetition number  $r$ .  $[G(q_{i+1}; q_i)]_{i+1, i}$  (with  $i, i+1 \in \{L, T\}$ ) is the Van-Vleck propagator (including instability factors, reflections and mode conversions [15]) if  $q_i$  and  $q_{i+1}$  are connected by a pure geometric trajectory, and  $\frac{i}{2} \mathcal{S}_R(!)_{i+1, i} \exp(i \dots)$  if  $q_i$  and  $q_{i+1}$  are the endpoints of a Rayleigh arc segment, with  $i, i+1$  the polarizations of the two attached geometric legs. The  $[\dots]_{i+1, i}$  diffraction matrix  $\mathcal{S}_R(!)$  is the elastodynamics analogue of the square of the corresponding QM diffraction constant [11,17,18]. It is determined by Keller and Karal [16] for the half-plane case, and in ref. [15] for the circular cavity.  $\mathcal{S}_R(!)_{i+1, i}$  is proportional to  $\exp[\dots]_{i+1, i}$  with  $(!)_{i+1, i} = R \text{arccosh}[R = (ak)] \frac{2}{R} (ak)^2$ , i.e., it is weakly attenuated for the pure shear case  $i+1 = i = T$ , but strongly attenuated otherwise.

The "semiclassical" form of the spectral determinant is given by the formal product  $\text{DetM}_{\text{geom}} : \text{DetM}_{\text{Rayl}}$ , evaluated in the cycle expansion where the classifying topological length is equal to the number of geometric straight legs of the orbits and pseudo orbits [2].

The Wigner time delays and cumulant traces are particularly well suited to detailed comparisons of the exact results with the SWA [11]. In Fig. 3 we plot the exact Wigner "time" delay  $c_l = \frac{d}{dk_L a} c_l(!) = \frac{1}{2} \ln \text{DetM}(!)^Y = \text{DetM}(!)$  as function of the pressure wave number  $k_L = ! = c_L$ , and compare it to the cycle expansion based on the geometric and complex periodic orbits of topological lengths one and two. The short-wavelength periodic orbit approximation is in good agreement with the exact cumulant expansion to second order. Finally, in Fig. 4 we compare the periods of the ray-dynamic periodic orbits with the Fourier peaks of the exact wave-mechanical data by plotting the moduli of the Fourier transforms of  $\text{Tr}A_{A_1}$  and  $\text{Tr}A_{A_1}^2$  for the region  $10 \leq k_L a \leq 45$ , and the corresponding Fourier transforms of sums over periodic orbits of topological length one and two, respectively. The Fourier peaks indeed correspond to the periodic-orbit periods  $T_p = \sum_{i_L} l_{i_L} = c_L + \sum_{i_T} l_{i_T} = c_T + \sum_{i_R} a_{i_R} = c_T$ , with  $l_{i_L}$ ,  $l_{i_T}$  and  $a_{i_R}$  the (effective) geometric lengths of the pressure, shear and Rayleigh segments, respectively.

The SWA captures nearly all qualitative features of the exact calculation. However, the  $1/k_L$  corrections are still not negligible, as can be seen from the small structure close to 0.1 m s in Fig. 4 (right). This corresponds to a combined LT geometric orbit that vanishes in the SWA, as there is no coupling of pressure to shear rays at perpendicular impact. The complex orbits visible in Fig. 4 have only shear segments coupled to Rayleigh segments, whereas the coupling of pressure segments to Rayleigh segments is severely suppressed (since  $c_L \ll c_R$ ). These

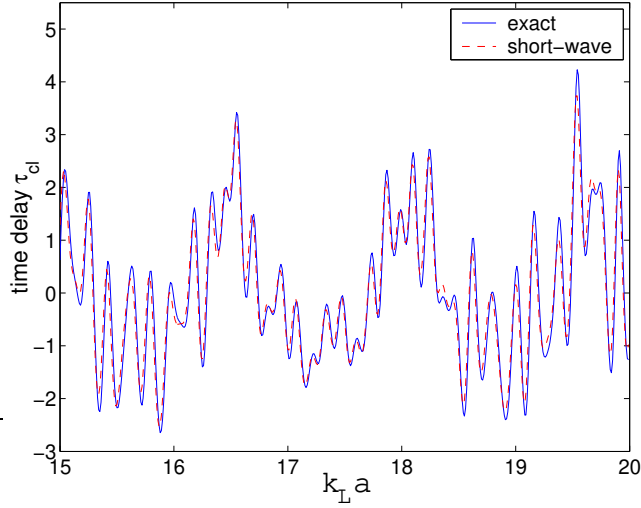


Fig. 3 { Wigner time delay for the two-cavity system, the exact  $A_1$  result versus its ray-dynamic expansion to period two, as function of the pressure wave number  $k_L$  (times the cavity radius  $a$ ).

observations explain the qualitative features of the low-energy resonance spectrum, g. 1: The chaotic band of the leading resonances arises from the interference of the exponentially growing number of Rayleigh orbits with the  $t_T$  orbit. The regular family of resonances in g. 1 at  $\text{Im } k_L = 0.29/a$  corresponds to the  $t_T$  orbit that dominates the QM case, but is subdominant here, masked by much narrower resonances arising from complex Rayleigh orbits.

Summary and outlook. { We have derived the scattering determinant and determined, in the low-energy regime, the exact scattering resonances and Wigner time delays for a quasi-two-dimensional isotropic and homogeneous elastodynamic slab with several cylindrical cavities.

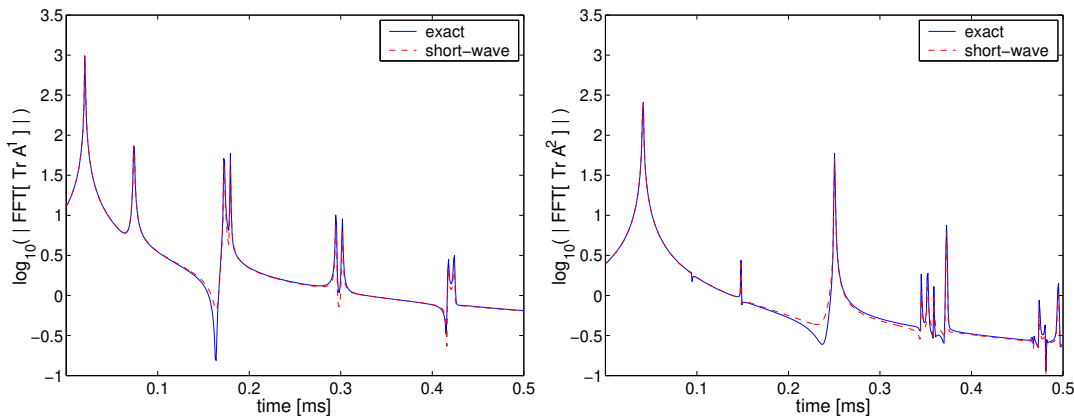


Fig. 4 { Comparison of the Fourier transforms of the exact traces  $\text{Tr} A_{A_1}$  (left panel) and  $\text{Tr} A_{A_1}^2$  (right panel) of the two-cavity system with the short-wavelength approximation (SWA) based on periodic orbits of topological length one and periodic orbits of topological length two, respectively, in the range  $10 < k_L a < 45$ . All peaks are identifiable as the periods of the shortest period orbits.

The physics of elastodynamic scattering with free boundary conditions is totally different from the physics of quantum billiards at low energies: almost all of the medium excitation resides in the weakly attenuated Rayleigh waves. The shear waves communicate between Rayleigh waves of differing cavities, with pressure waves only playing a secondary role.

A symbolic dynamics here needs to account for cycles patched together from four kinds of segments: pressure, shear, anti- and clockwise Rayleigh, implying an exponentially growing number of interfering periodic orbits. Contrary to QM two-cavity scatterers, the highly irregular elastodynamic resonance spectrum of  $g.1$  arises from the underlying chaotic repeller spanned by the increasing number of weakly attenuated complex periodic orbits of Rayleigh type. It is an open problem whether the topological increase or the attenuation of these orbits will win, i.e., whether the irregular band of "chaotic" resonances of  $g.1$  stays above the geometric resonances for  $k_L = 45a$ . Note that at  $k_L = 32a$  an additional band of resonances, which results at cumulant order 3 and 4, joins and starts to reshape the irregular one. Similar phenomena were observed in the QM spectrum of the classically chaotic three-disk system [11]. Thus additional band mergers at even larger  $k_L$  values would be a promising signal.

Numerically, the short-wavelength estimates and the exact Wigner time delays for the two-cavity system are in good agreement already in the second order of the cumulant expansion. The surprise is that that surface orbits of Rayleigh type - with no counterpart in QM - dominate the displayed low-energy spectrum.

Similar orbits are expected in general non-convex elastic resonators. Generalizations to anisotropic media (the highest  $Q$ -value experiments are performed on single crystals of quartz), and applications of the above ray-dynamics techniques to resonator geometries used in experiments remain open problems.

## REFERENCES

- [1] Gutzwiller M. C., *Chaos in Classical and Quantum Mechanics* (Springer, New York) 1990.
- [2] Cvitanovic P. et al., *Chaos: Classical and Quantum* (ChaosBook.org, Niels Bohr Inst., Copenhagen) 2004.
- [3] Ellegaard C., Guhr T., Lindemann K., Nygard J. and Oxenborow M., *Phys. Rev. Lett.*, 77 (1996) 4918.
- [4] Graf H.-D. et al., *Phys. Rev. Lett.*, 69 (1992) 1296.
- [5] Alt H. et al., *Phys. Rev. Lett.*, 74 (1995) 62.
- [6] Neicu T. and Kudrolli A., *Europhys. Lett.*, 57 (2002) 341.
- [7] Izbicki J. L., Conoir J. M. and Veksler N., *Wave Motion*, 28 (1998) 227.
- [8] Berry M. V., *Ann. Phys. (N.Y.)*, 131 (1981) 163.
- [9] Gaspard P. and Rice S. A., *J. Chem. Phys.*, 90 (1989) 2225; 90 (1989) 2242; 90 (1989) 2255.
- [10] Wirzba A., *CHAOS*, 2 (1992) 77; *Nucl. Phys. A*, 560 (1993) 136.
- [11] Wirzba A., *Phys. Reports*, 309 (1999) 1.
- [12] Landau L. D. and Lifshitz E. M., *Theory of Elasticity* (Pergamon, Oxford) 1959.
- [13] Couchmann L., Ott E. and Antonsen, Jr. T. M., *Phys. Rev. A*, 46 (1992) 6193.
- [14] Franz W., *Z. Naturforschung*, 9a (1954) 705.
- [15] Sndergaard N., *Wave Chaos in Elastodynamic Scattering* (PhD thesis, Northwestern Univ., Evanston) 2000; [www.nbi.dk/~nsonderg](http://www.nbi.dk/~nsonderg).
- [16] Keller J. B. and Karal, Jr. F. C., *J. Acoust. Soc. Am.*, 36 (1964) 32.
- [17] Vattay G., Wirzba A. and Rosenqvist P. E., *Phys. Rev. Lett.*, 73 (1994) 2304.
- [18] Rosenqvist P. E., Vattay G. and Wirzba A., *J. Stat. Phys.*, 83 (1996) 243.